

DOI: <https://doi.org/10.24425/amm.2024.147810>AIYONG CUI^{1*}, HAODONG LIU¹, SHAODONG GAO², HUAKAI WEI¹, JIALEI ZHAO²

LASER WELD SEAM CURVED PATH EFFECT ON 6063 ALUMINUM ALLOY STRENGTH AND TEMPERATURE DISTRIBUTIONS: COMSOL NUMERICAL SIMULATION

To improve the welding performance of aluminum alloys, a thermal source model of an irregular weld seam was established. COMSOL software was used for numerical simulation of the weld seam geometry effect on the temperature and stress fields in laser welding, which results were experimentally validated. The results show that the ellipsoidal laser welding melted micropool exhibited quasi-steady-state temperature field characteristics. The temperature gradient and thermal stress showed an increase followed by a decline. The temperature fluctuation amplitude of the square-tooth-shaped weld seam exceeded that of the arc-tooth-shaped one. The temperature evolution of the broken line tooth-shaped weld seam showed a slightly increasing trend, except for the inflection point. The experimental average tensile strength of the weld seam was the highest, reaching about 210 MPa, i.e., roughly 85% of the base material (245 MPa), which coincided with the COMSOL-based temperature field simulation results. With increasing deformation amplitude and transition radius, the maximum tensile force, tensile strength, and elongation at fracture showed an increasing trend. However, the deformation amplitude should be below a certain limit because its increase elongates the welding path and reduces the distance between weld seams, resulting in serious heat accumulation. The tensile fracture morphology of the 6063-T6 base material was curved shear, with shallow toughness pits, small tearing edges at the edges, and small granular objects, indicating small plastic deformation during the fracture process. The tensile fracture of the welded part spanned the weld seam and the base material, and the fracture occurred along the tangent direction of the weld seam. The fracture surface was smooth, the tearing edges at the edge of the toughness pit shifted along the weld seam direction, forming many co-directional slip bands, with highly pronounced plastic deformation.

Keywords: 6063 aluminum alloy; laser welding; irregular weld seam; COMSOL numerical simulation; mechanical properties

1. Introduction

The 6063-T6 aluminum alloy has a small density, good mechanical properties, excellent thermal processing, and corrosion resistance, implying its wide use in aerospace applications, including aircraft intakes and fuel tanks [1-4]. However, fatigue cracks and other defects in aerospace thin-walled aluminum alloy structures inevitably appear during their service due to the combined effects of cyclic loads, impact vibrations, corrosion, temperature differences, and other factors that seriously affect flight safety. Due to the special structure, small space, and difficulty accessing both sides of the aircraft intake and fuel tank, traditional riveting repair processes are not applicable, and alternative repair technologies are urgently needed. As an emerging joining technology, welding, especially laser welding, is increasingly accepted by the aerospace industry worldwide and has become a research hotspot [5-8]. However, the high

thermal conductivity, reflectivity, and element burnout combined with low welding stability make it difficult for linear welds of aluminum alloys produced by low-power lasers to meet strict quality requirements [9-13].

The research goal is to provide a new technology to replace riveting for the welding and repair of aluminum alloy structure damage on the surface of the aircraft, and to improve the performance of aluminum alloy structural welds with new ideas, so that the tensile strength in the direction of the main stress after welding and repair can reach the level of more than 85% of the strength of the base metal. Alternatively, weld seams made by curved laser paths provide strength re-distribution in the tensile/bending planes with mixed high-strength base and lower-strength weld materials. To this end, this study simulated various-shaped laser weld seams in 6063 aluminum alloy sheets using the finite element method run via COMSOL software. Numerical simulation and experimental laser welding tests were conducted to

¹ NAVAL AERONAUTICAL UNIVERSITY, QINGDAO, 266041, CHINA

² LIAONING UNIVERSITY OF TECHNOLOGY, JINZHOU, 121001, CHINA

* Corresponding e-mail: caylaser@163.com



clarify the effects of the weld seam geometry and size parameters on the temperature and stress fields of 6063 aluminum alloy plate subjected to laser welding. The study was aimed at improving the weld repair quality and providing theoretical support for the engineering application of low-power laser welding technology for damage repair of aluminum alloy parts.

2. Experimental materials and methods

The study used 6063-T6 aluminum alloy sheets with 100 mm × 60 mm × 3 mm dimensions. Their chemical composition is shown in TABLE 1. The laser power ranged from 1000 to 1200 W, the scanning speed ranged from 850 to 1250 mm/min, and the argon gas protection pressure ranged from 0.2 to 0.3 MPa. The welding was done on one side with a copper plate as a backing, and the defocus amount was -1 mm.

TABLE 1
Chemical composition of 6063-T6 aluminum alloy (at.%)

Si	Fe	Cu	Mn	Mg	Cr	Zn	Ti	Al
0.2-0.6	≤0.35	≤0.1	≤0.1	0.45-0.9	≤0.1	≤0.1	≤0.1	margin

A WD-P6205 universal testing machine was used to test the tensile strength. A Hitachi S-3400 N scanning electron microscope was applied to observe the fracture morphology; To design the structural model of different kinds of welds, the matrix is spliced together by two aluminum alloy plates, the size is 200 mm × 60 mm × 3 mm, and the weld position is located in the middle of the two plates, and with the help of COMSOL software, according to the actual material size, the model size is constructed, the curved weld is located in the middle position, the heat source travels in the direction of the curved weld, and the meshing of the loading surface of the heat source at the curved weld adopts a quadrilateral grid. The finite element method uses a numerical approximation to calculate, so in most cases, the more precise the meshing, the more accurate the final

result. Therefore, in order to increase the accuracy, the mesh accuracy level is ultra-fine on the heat source loading surface. a finite element model and path model were established for three irregular (rectangular, circular, and zigzag) weld path configurations depicted in Fig. 1, producing square tooth, arc tooth, and broken line shapes, respectively.

3. Experimental results

3.1. Temperature and stress fields of different-shaped weld seams

For the above three weld path configurations, the laser welding temperature evolution curves were experimentally obtained for monitoring points 1 to 13 depicted in Fig. 2 and plotted in Fig. 2(b-d).

As seen in Fig. 2a, the peak temperature fluctuation of the square tooth weld was not significant, reaching above 1100°C. Still, the peak and the valley have a large temperature difference. Although the bottom temperature of the valley showed a slow upward trend, the first half was still below the melting point of the base material, resulting in incomplete penetration on one side. The temperature fluctuation range of the arc tooth weld was smaller than that of the square tooth shape, and it was more stable, showing an upward trend. Still, the bottom temperature of the valley was mostly lower than the melting point of the base material. In the straight line section of the broken line tooth weld, the temperature was higher, with a peak temperature exceeding 1100°C, and the bottom temperature of the weld was over 800°C, exceeding the melting point of the base material. Despite a significant temperature drop at turning points 1 (4, 5, 6) and 2 (8, 9, 10), the peak temperature was still above 900°C, while all temperature curves were stable and slightly rising. The broken line tooth weld temperature evolution was the most regular, and the respective welding process was the most controllable.

The temperature distribution law of laser welding is shown in Fig. 3. As the heat source of laser welding moved, the basic

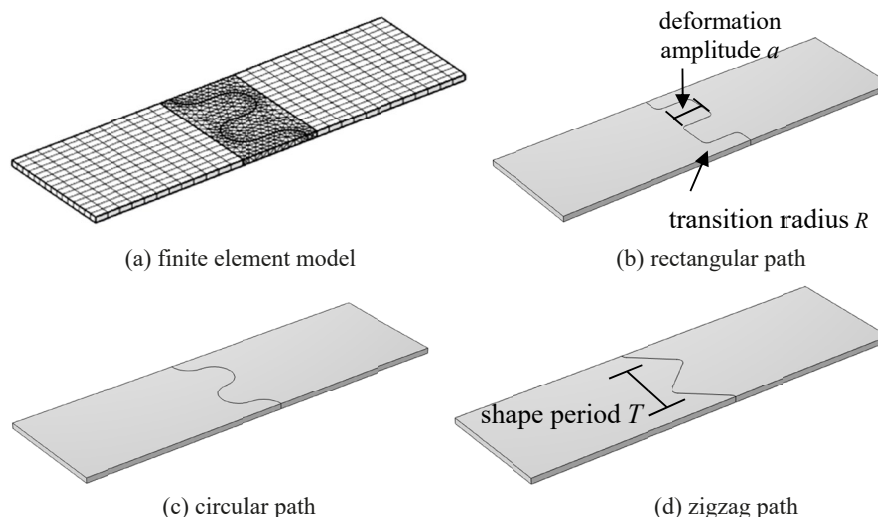


Fig. 1. Curve path simulation model

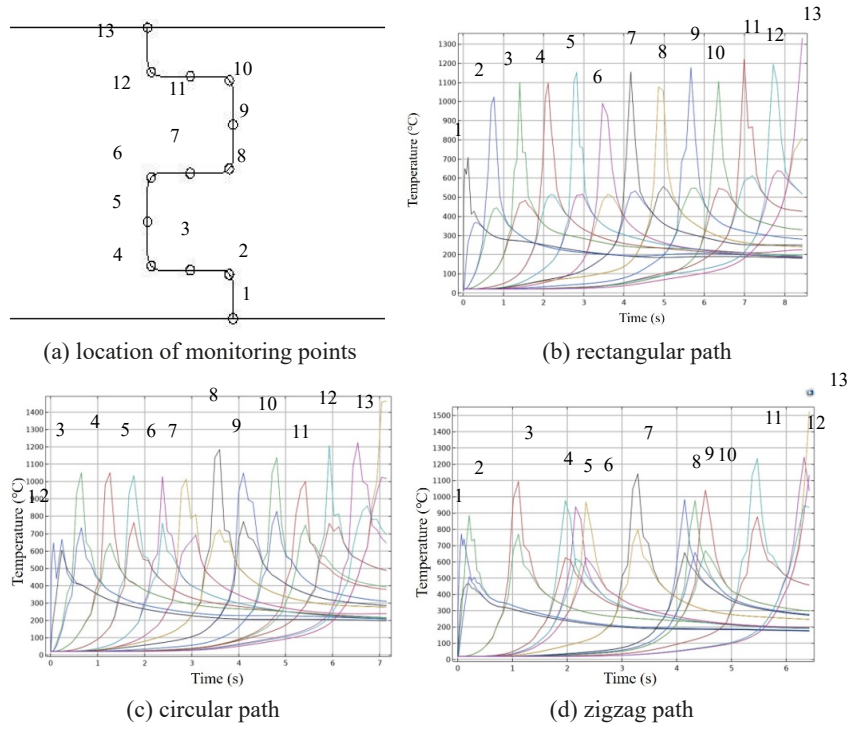


Fig. 2. Temperature-time curve of different curve paths

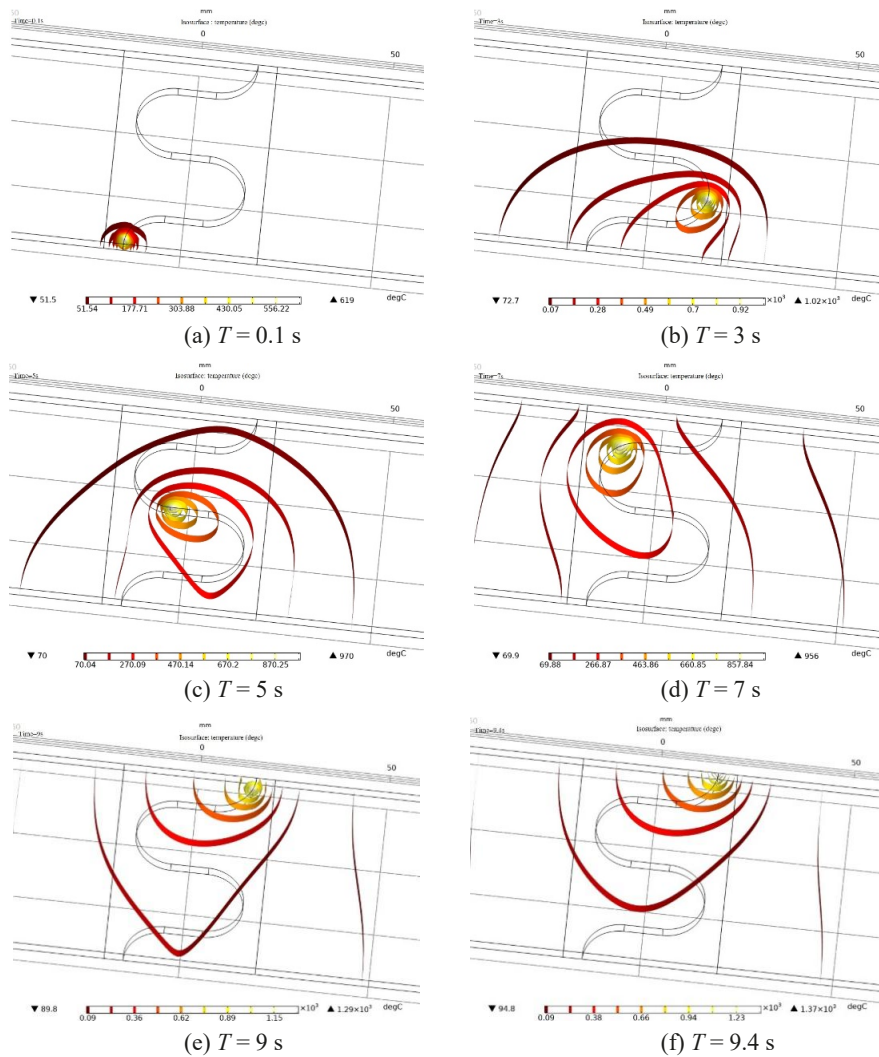


Fig. 3. Temperature field at different times

shape of the welding pool did not change and remained elliptical, showing quasi-steady-state temperature field characteristics. The temperature field distribution gradually changed from the initial approximate semi-elliptical arc tooth shape to an elliptical one, and the temperature lines showed a semi-circular arc divergent shape. They also varied with time, gradually becoming less dense, indicating a decreasing trend in the temperature gradient.

The initial condition of the weldment is the distribution of the temperature field at the initial time, and the initial temperature before the simulation is set to 293K. The thermal radiation phenomenon has little influence on this simulation, so only the deformation and stress in the thermal convection laser welding process are considered. The influence of temperature gradient changes on the stress field of laser welding is shown in Fig. 4. When the heat source was applied to the welding starting point, there was no constraint on the solidification section of the weld, so the thermal stress was relatively small. With the increased length of the solidified weld and increased thermal accumulation, the tensile stress formed by the coupling effect of temperature and constraint force grew rapidly, promoting formation of such

defects as thermal cracks, pores, and collapse. At the end of the weld seam, the thermal accumulation reached a high level, the overall temperature of the base material increased, the temperature gradient dropped, while the thermal stress showed a downward trend.

3.2. Tensile properties of different shaped welds

This study adopted the deformation amplitude $a = 20$ mm, shape period $T = 40$ mm, and transition radius $r = 3$ mm. The tensile performance curves of three different-shaped welds are shown in Fig. 5.

The average tensile strength of the zigzag weld was the highest (150 MPa), with a maximum value of 154 MPa and a minimum value of 145 MPa), surpassing that of the square tooth and arc tooth welds (with maximum, minimum, and average values of 136, 84, and 114 MPa, respectively). These results were consistent with the temperature field simulation results of COMSOL.

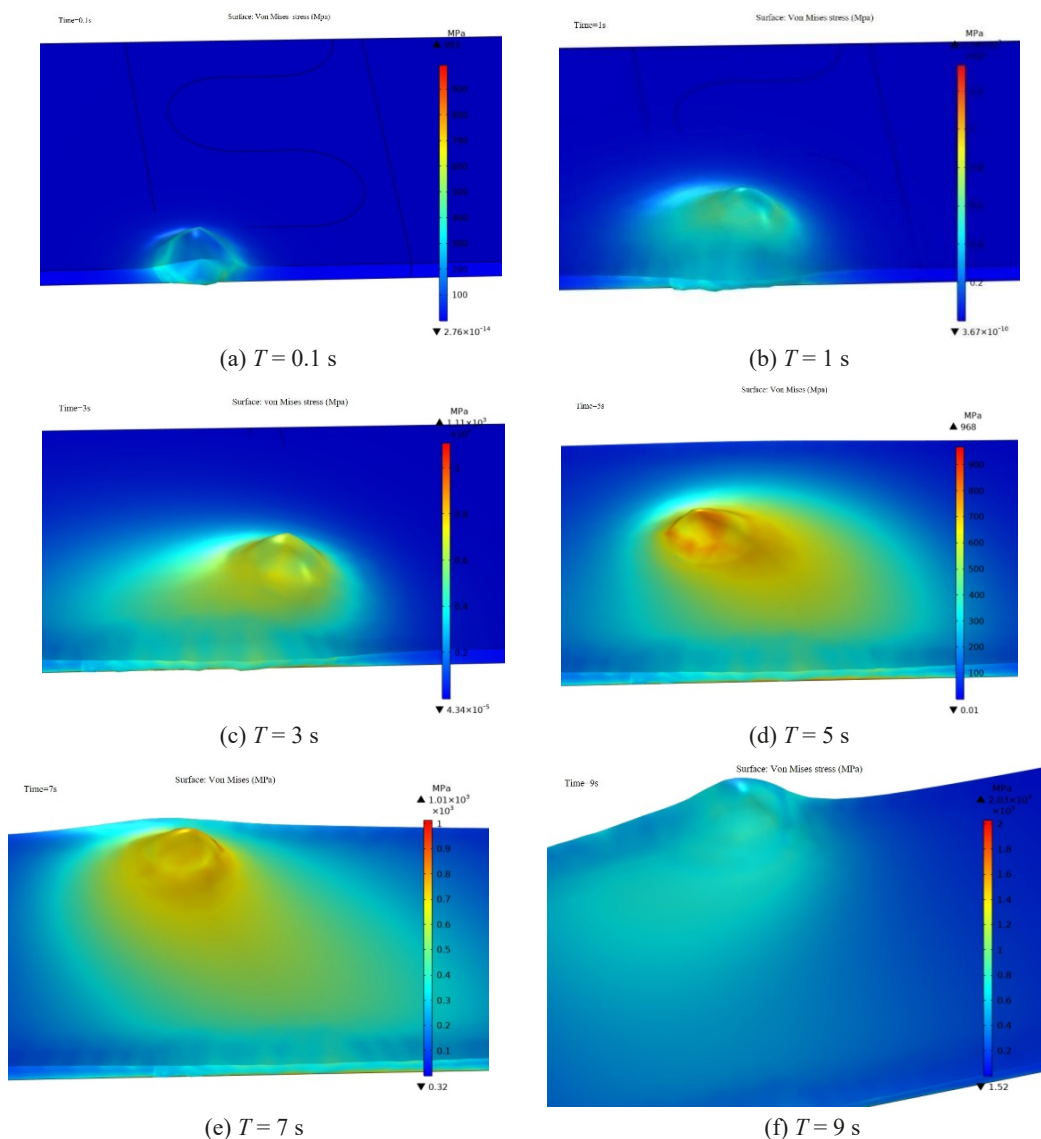


Fig. 4. Thermal stress distribution at different time locations under the same group of paths

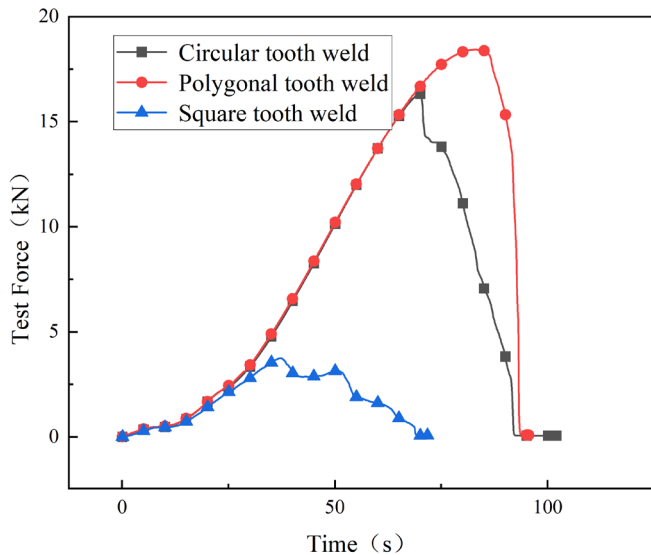
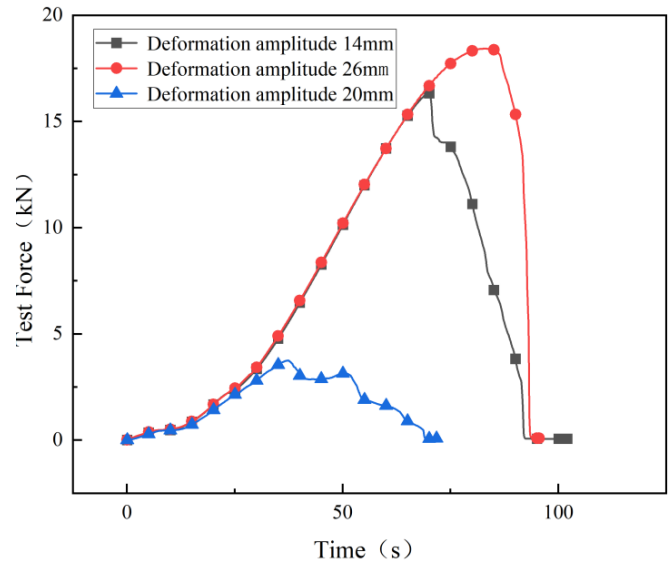


Fig. 5. Force-time curve of the curve path tensile test ($a = 20$ mm, $T = 40$ mm, $r = 3$ mm)

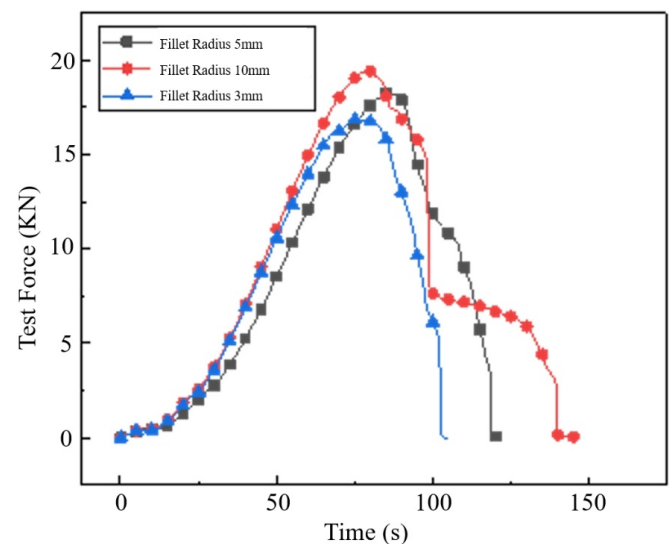
At the turning point, the operation was hindered, the dwell time increased, and such phenomena as excessive temperature of the base material, collapse of the weld seam, and even melting might occur, affecting the forming quality and reducing the mechanical properties. Therefore, the deformation amplitude a and transition radius r of the zigzag tooth weld seam were optimized, as shown in Fig. 6.

It can be seen that with the increase in the deformation amplitude and transition radius, the maximum tensile force, tensile strength, and elongation at break all showed an upward trend, with a maximum tensile strength of approximately 210 MPa, reaching 85% of the base material (245 MPa). Suitable shape parameters could effectively improve the welding performance, but the deformation amplitude should be kept within certain limits, because excessive amplitude will lengthen the welding path, reduce the distance between weld seams, and result in severe heat accumulation.

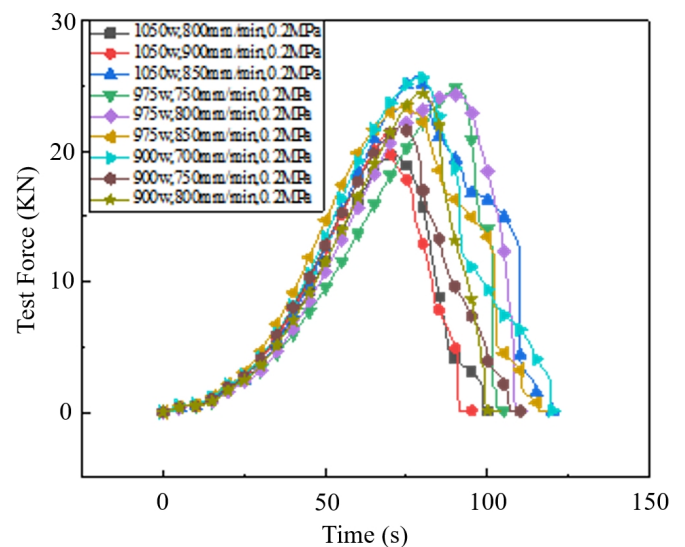
The tensile fracture morphology of the 6063-T6 substrate is shown in Fig. 7a, which appears as a curved shear shape with a shallow notch depth. There are small tearing edges at the edges and small granular objects around, indicating that the plastic deformation generated during the fracture process is small. Many holes at the fracture surface are prone to stress concentration and microcracks, reducing plasticity. Tensile fracture of the welded part occurs in the weld zone and the original material zone, as shown in Fig. 7b. At point A, due to the presence of porosity defects, the notch depth of the fracture increases significantly, there are small voids around, and the tearing edges at the edges are smaller than those of the substrate, indicating a decrease in stress and a decrease in plasticity and toughness during the tensile process. At point B, the fracture occurs along the tangent direction of the weld, the fracture surface is smoother, and the tearing edges at the notch are offset along the direction of the weld, forming a large number of slip bands in the same direction, which is a typical characteristic of plastic deformation [14].



(a) Different deformation amplitudes ($r = 3$ mm)



(b) Different fillet radii ($a = 30$ mm)



(c) Different process parameters ($P = 975$ W, $V = 800$ mm/min)

Fig. 6. Force evolution curves for different deformation amplitudes (a), fillet radii (b), and process parameters (c)

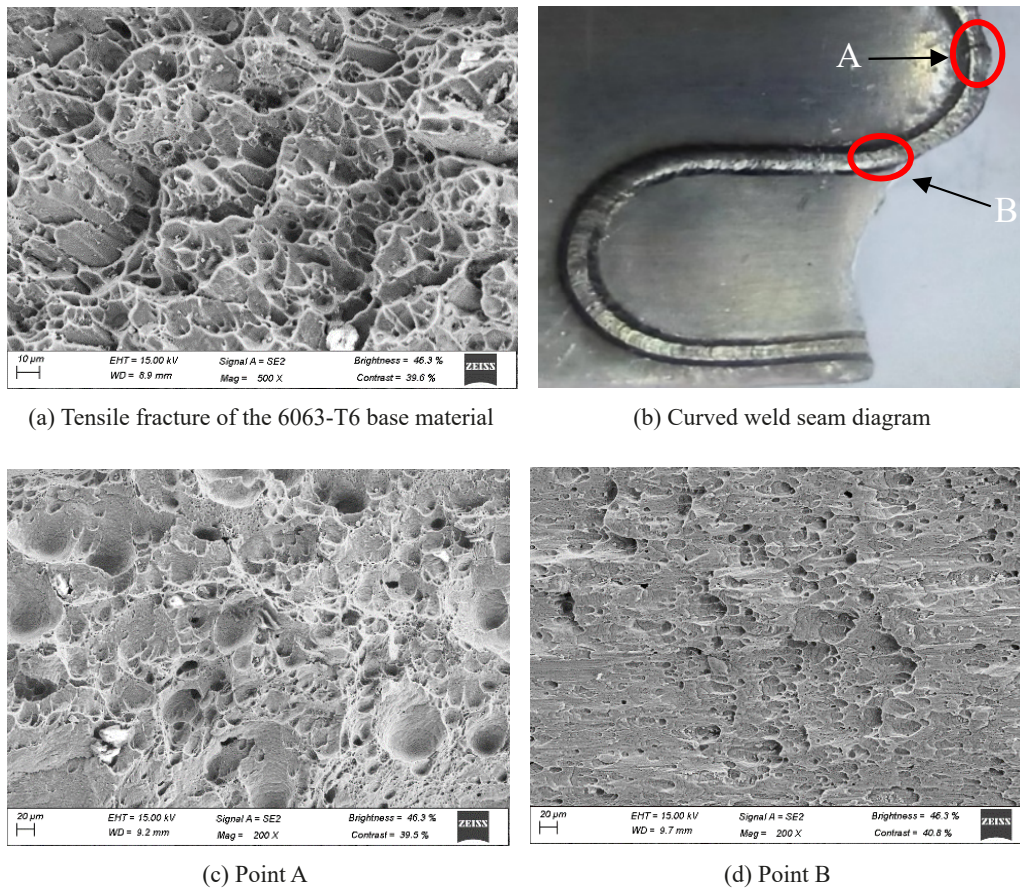


Fig. 7. SEM images of the tensile fracture of the weld and 6063-T6 alloy

4. Conclusions

The results obtained made it possible to draw the following conclusions:

- (1) The melted micropool in laser welding remains elliptical in shape and exhibits a quasi-steady-state temperature field. The temperature field distribution gradually changes from an initial approximate semielliptical arc tooth shape to an elliptical shape. The temperature lines show a semi-circular arc divergent shape, which changes over time. The temperature lines gradually change from dense to sparse, indicating a decreasing trend in the temperature gradient. The thermal stress shows an initial increase followed by a decreasing trend.
- (2) The temperature of the square tooth weld seam fluctuates unstably; the temperature fluctuation amplitude of the arc tooth weld seam is smaller than that of the square tooth; except for the turning point, the temperature of the broken line tooth weld seam is in a stable and slightly rising state, and the average tensile strength of the weld seam is the highest, reaching approximately 210 MPa, i.e., 85% of the base material (245 MPa), which is consistent with the temperature field simulation results of COMSOL.
- (3) Appropriate shape parameters can effectively improve welding performance. With the increase in deformation amplitude and transition fillet radius, the maximum tensile force, tensile strength, and elongation after fracture all show

an upward trend. However, the deformation amplitude should be limited. Increasing the amplitude will lengthen the welding path, decrease the distance between welds, and result in severe heat accumulation.

- (4) The tensile fracture morphology of the 6063-T6 substrate is curved and sheared, with a shallow notch depth and small tearing edges at the edges. Small granular objects nearby indicate that the plastic deformation generated during the fracture process is small. The tensile fracture of the welded part spans the weld and the base material, and the fracture occurs along the tangent direction of the weld. The fracture surface is smooth, and the tearing edges at the notch are offset along the weld direction, forming numerous co-directional slip bands with obvious plastic deformation characteristics.

REFERENCES

- [1] W. Tao, S.L. Yang, Application status and development trend of aluminum alloy laser welding. *MW Metal Forming* (2), 1-4 (2021).
- [2] Y. Wei, Influence of aging time on the microstructure and mechanical properties of the 6063 aluminum alloy for automobiles. *Hot Working Technology* 49 (14), 134-136 (2020).
- [3] F.J. Dind, Application of the aluminum alloy in photovoltaic bracket. *Light Alloy Fabrication Technology* 47 (10), 11-13 (2019).

- [4] J.Y. Liu, R.P. Jiang, X.Q. Li, Cracking failure analysis of the 7A09 aluminum alloy hydraulic cylinder. *Hot Working Technology* **48** (13), 164-167 (2019).
- [5] F.C. Ren, X. Liang, X.H. Wu, Cracking failure analysis of the aluminium alloy escalator steps. *Heat Treatment of Metals (S1)*, 286-289 (2019).
- [6] W. Duan, L.H. Zhou, Simulation study of laser welding of aluminum alloy plate based on Simufact. welding, *Hot Working Technology* **15**, 168-171 (2018).
- [7] W.W. Zheng, Numerical simulation of the stress-strain field in laser welding based on SYSWELD. *Journal of Mechanical Engineer* **328** (10), 74-76+79 (2018).
- [8] Y.B. Chen, S.X. Xu, S.Q. Tan, S.C. Song, Study on laser welding of aluminum alloys. *Modern Manufacturing Technology and Equipment* (8), 36-37 (2020).
- [9] Y. Kang, X.H. Zhan, X.S. Feng, P.Y. Xia, Numerical simulation study on temperature field and stress-strain field of 6061 aluminum alloy in laser beam welding. *Aerospace Shanghai* **6** (58-63), **37** (06), 58-63+68 (2020).
- [10] D.M. Li, Z.M. Li, X.F. Sun, W. Song, P. Song, B.J. Zheng, Research status and prospect of laser welding for low alloy high strength steel. *Transactions of Materials and Heat Treatment* **41** (11), 1-10 (2020).
- [11] Y.L. Xu, C.R. Li, J.Y. Li, M.X. Shi, Influence of process parameters on the microstructure and properties of laser welded joints of the 6061-T6 aluminum alloy. *Hot Working Technology* 1-6 (2022).
- [12] D. Liu, Evaluation of mechanical and forming properties of the laser welded joints of the 6063 aluminum alloy. Ph. D. Thesis, Qinhuangdao, Yanshan University, 2021.
- [13] H.D. Liu, F.Y. Hu, G.Q. Lei, F. Huang, A.Y. Cui, Analysis of welding tests of the LY12 aluminum alloy based on fiber laser. *Welding Journal* (7), 25-30 (2017).
- [14] C.G. Fan, S.L. Yang, C.F. Duan, M.Q. Zhu, Y.S. Bai, Microstructure and mechanical properties of 6061 aluminum alloy laser-MIG hybrid welding joint. *Journal of Central South University* **29** (3), 898-911 (2022).